The Journal of Chemical Physics

Optical and electronic properties of silver nanoparticles embedded in cerium oxide

Cite as: J. Chem. Phys. **152**, 114704 (2020); https://doi.org/10.1063/1.5142528
Submitted: 14 December 2019 . Accepted: 24 February 2020 . Published Online: 17 March 2020

Jacopo Stefano Pelli Cresi, Enrico Silvagni, Giovanni Bertoni, Maria Chiara Spadaro, Stefania Benedetti, Sergio Valeri, Sergio D'Addato, and Paola Luches

The Journal of Chemical Physics ARTICLE scitation.org/journal/jcp

Optical and electronic properties of silver nanoparticles embedded in cerium oxide

Cite as: J. Chem. Phys. 152, 114704 (2020); doi: 10.1063/1.5142528
Submitted: 14 December 2019 • Accepted: 24 February 2020 •
Published Online: 17 March 2020

Jacopo Stefano Pelli Cresi,[1,2] Enrico Silvagni,[1] Giovanni Bertoni,[2,3] Maria Chiara Spadaro,[1,2] Stefania Benedetti,[2] Sergio Valeri,[1,2] Sergio D'Addato,[1,2] and Paola Luches[2,a)]

AFFILIATIONS

[1] Dipartimento di Scienze Fisiche Informatiche e Matematiche, Università degli Studi di Modena e Reggio Emilia, Via G. Campi 213/a, 41125 Modena, Italy

[2] Istituto Nanoscienze, Consiglio Nazionale delle Ricerche, Via G. Campi 213/a, 41125 Modena, Italy

[3] Istituto dei Materiali per l'Elettronica e il Magnetismo, Consiglio Nazionale delle Ricerche, Parco Area delle Scienze 37/a, 43124 Parma, Italy

Note: This article is part of the JCP Special Topic on Oxide Chemistry and Catalysis.
[a)] **Author to whom correspondence should be addressed:** paola.luches@nano.cnr.it

ABSTRACT

Wide bandgap oxides can be sensitized to visible light by coupling them with plasmonic nanoparticles (NPs). We investigate the optical and electronic properties of composite materials made of Ag NPs embedded within cerium oxide layers of different thickness. The electronic properties of the materials are investigated by x-ray and ultraviolet photoemission spectroscopy, which demonstrates the occurrence of static charge transfers between the metal and the oxide and its dependence on the NP size. Ultraviolet-visible spectrophotometry measurements show that the materials have a strong absorption in the visible range induced by the excitation of localized surface plasmon resonances. The plasmonic absorption band can be modified in shape and intensity by changing the NP aspect ratio and density and the thickness of the cerium oxide film.

INTRODUCTION

In recent years, research activities on active catalysts for environmental protection have gained an increased relevance and urgency also due to the widespread concern for global warming.[1] Cerium oxide based catalysts are active in a number of important environmental reactions, the most successful commercial applications being in car catalytic converters and in antiparticulate filters for diesel engines.[2] More recent applications of cerium oxide based materials include fuel cell electrodes[3,4] and catalysts for the synthesis of solar fuels.[5] However, the application of cerium oxide based materials as photocatalysts is limited by the CeO_2 bandgap in the ultraviolet (3.2–3.6 eV)[6] and by the relatively low electron mobility of the material.[7] Methods to sensitize cerium oxide based materials to visible light include nanostructuration,[8–10] defect engineering,[11] doping,[12,13] and the coupling with metallic nanoparticles (NPs), for example, Au or Ag.[10,12,14–16] In the latter case, visible light excites the so-called localized surface plasmon resonances (LSPR) within the NPs. The energy of such resonant excitations can be transferred to the neighboring oxide modifying its properties and its catalytic activity.[14,16] The interaction between the NPs and the oxide after LSPR excitation may involve different mechanisms. Direct energy transfers and direct or indirect charge transfer processes may occur.[17–19] Indeed, the specific processes which can take place and their efficiency depend on various characteristics of the investigated materials, for example, the dielectric environment of the NPs, their size, shape and density, the atomic scale structure of the interfaces, the alignment of the energy bands of the oxide and of the metal NP, and the Schottky barrier which is formed between the two materials. The need for a design-driven synthesis of efficient photocatalytic materials calls for accurate studies of the involved materials in terms of the above-mentioned parameters.

Static charge transfer processes,[20–23] as well as more complex interaction mechanisms,[24–26] have been identified on model systems made of metal NP supported on cerium oxide surfaces. The influence of such processes on the functionality of the composite

materials has been recognized, although the resulting optical properties are comparatively less understood.

Among the investigated metal NPs, Ag has the advantage of having a strong absorption cross section in the visible range and of being relatively less critical than, for example, Au or Pt in terms of availability and cost. Composite systems made of Ag NPs embedded within cerium oxide matrixes have recently been investigated and a long-living and efficient plasmon-mediated charge transfer has been hypothesized, based on the results of fast transient absorption spectroscopy.[27] Moreover, a superior LSPR-induced catalytic activity of Ag/CeO_2 systems under visible light irradiation was recently demonstrated.[12,28]

Metals deposited by physical methods on oxide surfaces typically self-assemble into nanoparticles, with the size and shape determined by the metal-oxide interaction, by the oxide surface morphology, and by the deposition temperature.[29] In most cases, both the NP size and/or their density tend to increase with the amount of deposited metal. Here, we present a systematic study of the electronic and optical properties of Ag NPs of different sizes and densities coupled with cerium oxide. The investigation provides important insights into the interaction between the two materials, important for a knowledge-driven design of cerium oxide based materials with a high efficiency toward visible light absorption.

EXPERIMENTAL

The samples investigated in this study are Ag NPs of variable size and density embedded within or supported on CeO_2 films. Double side polished MgO(001) single crystals were chosen as supports for the Ag NPs–CeO_2 systems since they ensure a good optical transparency in the visible range. The substrates were cleaned by two subsequent ultrasonic baths in warm (373 K) acetone and in isopropanol for 5 min and introduced in an ultra-high vacuum apparatus for further cleaning by heating at 673 K for 30 min. Cerium oxide films of different thickness were grown by reactive molecular beam epitaxy (MBE), by evaporating Ce, using an electron beam cell, in an oxygen partial pressure of 1×10^{-7} mbar on the MgO substrate kept at room temperature (RT). The Ag NPs were self-assembled on the cerium oxide film surface at RT by depositing Ag from a Knudsen cell. Both the Ce and Ag evaporators were calibrated by a quartz crystal microbalance. The size and density of the Ag NPs obtained depend on the amount of Ag deposited. We have focused the present study on NPs formed by depositing 2 Å, 4 Å, and 12 Å of Ag on the cerium oxide film surface, where the nominal Ag amount refers to the equivalent thickness of a uniform Ag layer fully covering the oxide surface. The samples for *ex situ* characterization were covered by a further cerium oxide layer to provide a dielectric environment also above the NP and to simultaneously protect the Ag NPs from contamination induced by air exposure. To increase the optical absorption of the 2 Å and 4 Å Ag NP sample, we grew multiple layers of Ag NPs, each containing the same Ag amount (2 Å or 4 Å), intercalated by CeO_2 films, each having the same thickness (0.5 nm, 1 nm, or 2 nm) as schematically shown in Fig. 1. All of the layers were grown at RT. We note that the real morphology of the investigated samples is far more complex than the one sketched in Fig. 1 and that the intermediate oxide layers may leave some of the largest NPs partially uncovered. Some of the Ag NPs belonging to subsequent layers may indeed be partly in contact (center and bottom panels). For the case of 4 Å Ag NPs, three different samples with NP layers intercalated by oxide layers of 0.5 nm, 1 nm and 2 nm thickness were prepared in order to investigate also the effect of the dielectric thickness on the optical properties (see Fig. 1). Pure CeO_2 films of different thicknesses without Ag NPs were also grown and measured for comparison.

The electronic properties of the samples were analyzed *in situ* by x-ray photoemission spectroscopy (XPS) and ultraviolet photoemission spectroscopy (UPS). For the XPS measurements, we used Al K_α photons from a double anode x-ray source and a hemispherical

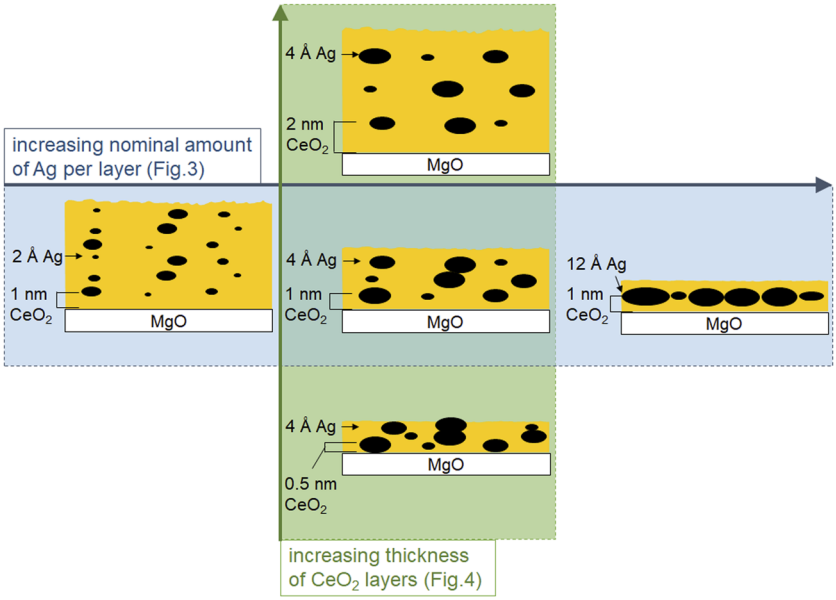

FIG. 1. Simplified cross-sectional sketches of the samples investigated by UV–Vis spectrophotometry.

electron analyzer in a normal emission geometry. The analysis of Ce 3d spectra is a powerful method to precisely determine the evolution of stoichiometry of the surface of cerium oxide based materials. The fitting of the spectra was performed using a procedure introduced by Romeo *et al.*[30] and further improved by Skala and co-workers,[31] which we have already used to evaluate the Ce^{3+} and Ce^{4+} concentration in a number of previous studies.[32,33] Briefly, it consists in fitting the spectra using five Voigt-shaped doublets, three related to photoemission from Ce^{4+} ions and two related to photoemission from Ce^{3+} ions with different final states. The procedure is relatively precise in detecting changes in the concentration of Ce^{3+} and Ce^{4+} in different samples, while the accuracy on the numbers obtained is affected by a relatively large error. The UPS measurements were acquired using a helium lamp and a hemispherical electron analyzer at normal emission.

The optical properties were investigated *ex situ* using an ultraviolet-visible (UV–Vis) spectrophotometer equipped with a xenon lamp, a grating monochromator, and a silicon photodetector (detection range 250–750 nm). The incidence angle between the incident photon beam and the sample normal was set to 22°. The absorbance A was evaluated by measuring the transmittance T and the reflectance R as $A = 1 - T - R$.

The morphology of the system was also investigated *ex situ* by scanning transmission electron microscopy (STEM), using a JOEL JEM-2200FS microscope located at CNR-IMEM in Parma, on a sample grown directly on a TEM grid (consisting in thin carbon films supported on a Cu mesh) with the same procedures used for the samples grown on MgO. The TEM was operated also with an energy dispersive x-ray spectrometer (EDXS) to determine the distribution of Ag and Ce on the sample surface.

RESULTS AND DISCUSSION

The morphology of the MBE-grown Ag NPs embedded between two CeO_2 layers was investigated by TEM. Figure 2(a) reports a representative annular dark-field scanning TEM (ADF-STEM) image of a portion of a 4 Å Ag NP sample embedded between two cerium oxide layers of 1 nm thickness.

The Ag particles appear bright in the image due to the higher average atomic number (about 1.5 times the CeO_2 value by averaging in the unit cell volume). The Ag size distribution, shown in Fig. 2(b), was measured from a series of images (using conventional particle analysis as implemented in the ImageJ software[34]). The size distribution is rather broad, it has a maximum around 3 nm, and the maximum NP diameter is ~10 nm. EDXS maps from the Ce-L edge (cyan) and Ag-L edge (magenta), shown in Fig. 2(c), confirm that Ag is concentrated into NPs, while cerium is uniformly distributed on the sample surface. A rough estimate of the aspect ratio of the NPs, defined as the ratio between the NP diameter and its height, can be obtained by evaluating the fraction of sample surface covered by Ag NPs from images like the one in Fig. 2(c). Since the nanoparticles cover ~25%–30% of the surface and the

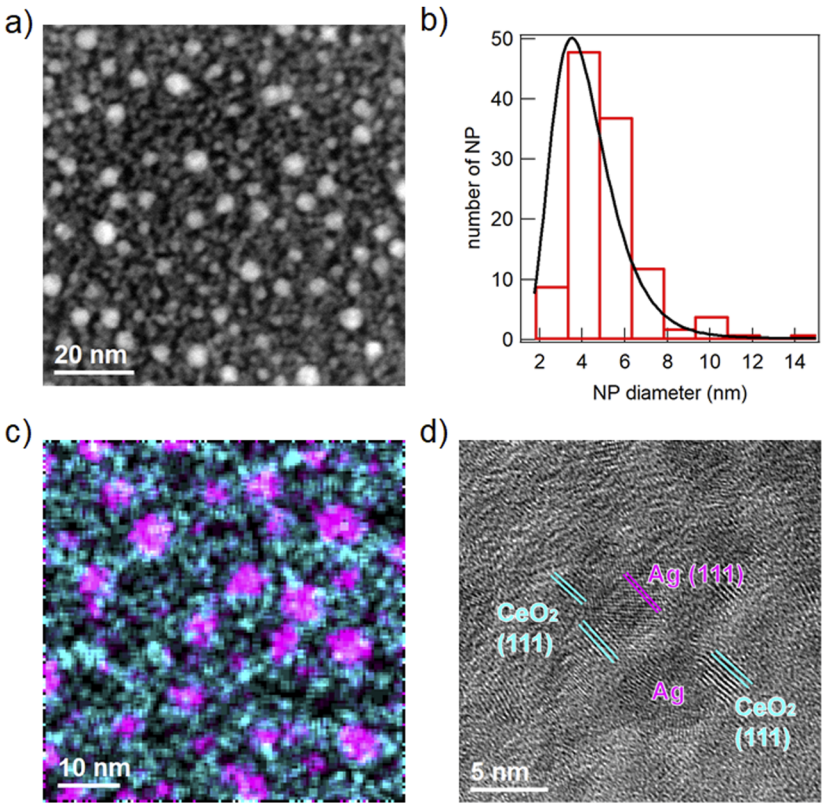

FIG. 2. (a) STEM image of the 4 Å Ag sample, (b) size distribution extracted from STEM images, (c) EDXS map of Ce L-edge intensity (cyan) and Ag L-edge (magenta) intensity, and (d) HRTEM in which some of the Ag(111) and CeO_2(111) planes are evidenced.

amount of Ag deposited is 4 Å, the average height of the Ag NPs is ~1.3–1.6 nm. Indeed, the aspect ratio is expected to depend on the size and shape adopted by the NPs. However, an estimate of the dominant aspect ratio for the 4 Å Ag sample can be obtained by considering that the largest fraction of the NPs have an in-plane size of 3 nm and a height of 1.3–1.6 nm, which give an aspect ratio of ~2 or higher. Figure 2(d) reports a high-resolution TEM (HRTEM) image acquired on the same sample, which demonstrates that most of the Ag nanoparticles have a polyhedral shape and a polycrystalline structure. Cerium oxide forms small crystalline domains with a lateral size of a few nm. In some cases, the oxide grains and the metal NPs show some mutual in-plane crystallographic alignment. This is evidenced in Fig. 2(d), which highlights CeO_2 (111) planes (d_1 = 3.12 Å) aligned parallel to Ag(111) planes (d_2 = 2.36 Å). Although the lattice mismatch between the CeO_2(111) and Ag(111) surface unit cells is rather large, cerium oxide grains have some tendency to align their most stable (111) facets with Ag NP (111) facets, in analogy with the case of cerium oxide films grown on (111) metal surfaces.[35–37]

Cerium oxide films deposited on polished MgO(001) surfaces and on TEM grids with the same procedures are expected to have a comparable roughness since polished oxide surfaces are not atomically flat and no simple epitaxial relation is expected to be established between the MgO(001) surface and the most stable low-index cerium oxide planes. Therefore, we expect the Ag NP morphology and structure to be comparable in the samples deposited on the two different substrates.

The size and shape of the NPs and, in particular, their aspect ratio, determine the energy of the optical absorption features.[38] Indeed, also the dielectric in which the NPs are embedded plays a relevant role in determining the polarizability and hence the dielectric response of the material. Moreover, the plasmonic resonance modes can be shifted by interparticle interactions.[39,40] We investigated the dependence of the optical response on the above-mentioned parameters in the case of the Ag NPs-CeO_2 system, by measuring the UV–Vis absorbance spectra as a function of Ag nominal thickness and as a function of the thickness of the CeO_2 film in which the Ag NPs are embedded. Figure 3(a) shows the UV–Vis absorbance spectra of 2 Å, 4 Å, and 12 Å Ag samples embedded within two ceria layers of a constant thickness of 1 nm. The 2 Å and 4 Å Ag samples consist of six and three repeated layers of Ag NPs, respectively (see Fig. 1). The spectra in Fig. 3(a) show a feature at ~275 nm, which is ascribed to transitions to defect states in the MgO substrate,[41] a second peak at ~320 nm, which corresponds to transitions from the d-like part of the valence band to the empty 4f levels in the CeO_2 matrix,[42] and a broad LSPR band in the visible range (the UV–Vis spectra of bare MgO and CeO_2/MgO are shown in the supplementary material). In order to compare the LSPRs-related features in the different samples, we considered the differential absorbance spectra, $\frac{\Delta A}{A} = \frac{A - A_{CeO_2}}{A_{CeO_2}}$, where A_{CeO_2} is the absorbance of a CeO_2 film without embedded Ag NPs. The resulting spectra, reported in Fig. 3(b), show an increasing intensity as the amount of Ag per layer is increased although the total amount of Ag is nominally the same in each sample. This is not surprising since the absorption cross section is proportional to the volume of the NPs, when the light wavelength is much larger than the NP size as in the case here investigated. The broad absorption feature in the visible range is composed by different peaks, one centered slightly above 400 nm, whose position appears unaltered in the different samples, and a second very broad feature at higher wavelengths, which significantly increases in intensity and progressively shifts toward higher wavelengths as the amount of Ag per layer is increased. The morphology of the

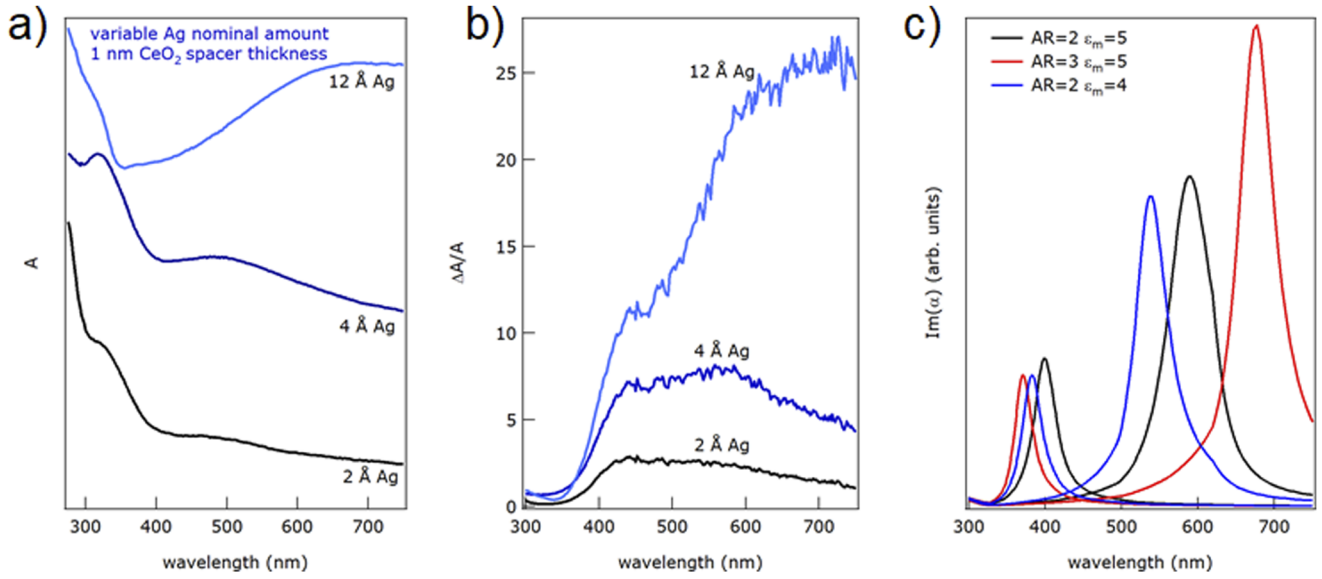

FIG. 3. (a) UV–Vis absorbance, (b) ΔA/A spectra of a 2 Å, 4 Å, and 12 Å Ag embedded within CeO_2 films of 1 nm thickness, (c) imaginary part of the calculated polarizability for Ag NPs of different aspect ratio embedded in a dielectric medium with different values of dielectric constant.

samples here investigated is quite complex, with relatively broad distributions of sizes and interparticle distances (Fig. 2). Broad LSPR absorption features at comparable wavelengths have already been identified in Ag NPs with a size of a few nanometers and ascribed to some anisotropy in their shape or environment.[27,43–45] In the case here investigated, an aspect ratio larger than one is expected due to nanoparticle substrate interactions.[21,46] To understand the evolution of the optical absorbance as a function of the amount of Ag deposited within each NP layer, we calculated the polarizability of the Ag NPs embedded in a CeO_2 matrix, using the Maxwell–Garnett model[47] with a dielectric function for Ag taken from Ref. 48 and a dielectric constant equal to 5 for CeO_2.[49] Following Ref. 50, we assumed Ag NPs with a spheroidal shape and a variable aspect ratio (see the supplementary material for details). The imaginary part of the polarizabilities derived within the model is shown in Fig. 3(c). An aspect ratio of 2, as estimated from the TEM images, splits the plasmon resonances into two peaks, an out-of-plane resonance around 400 nm, and an in-plane resonance around 590 nm. Figure 3(c) also shows that an increase of the aspect ratio to three induces a red shift of the in-plane component to 680 nm, while the out-of-plane component is only mildly blue-shifted. A decrease of the dielectric constant to 4, which may account for the finite thickness of the dielectric medium,[50] instead, blue-shifts the in-plane component. Moreover, in-plane interparticle interactions, which are not considered in the calculations, are expected to red-shift the in-plane LSPR, when the mutual distance between two NPs is smaller than a few nm.[39,40] These effects can explain the observed increases in absorbance at high wavelengths as a function of the nominal Ag thickness, i.e., with increasing Ag NP density [Fig. 3(b)]. The NPs are in fact expected to be progressively denser and to possibly have a slightly larger aspect ratio, which can result in a higher weight of the red-shifted in-plane resonance. The distribution in size and aspect ratio of the NPs and the possible deviations of the dielectric constant of the medium from the bulk value due to the finite film thickness can explain the broadness of the observed features.

To have more information on the optical properties of Ag NPs coupled with CeO_2, we also investigated the evolution of the absorbance spectra in three samples with a fixed amount of Ag NPs per layer (4 Å) separated by CeO_2 layers of 0.5 nm, 1 nm, and 2 nm thickness, respectively (see Fig. 1). The three samples consist of three repetitions of Ag NP layers. The UV–Vis spectra and the corresponding $\frac{\Delta A}{A}$ spectra are reported in Fig. 4. In Fig. 4(a), we can clearly see that the feature corresponding to CeO_2 interband transitions at 320 nm has a progressively increasing intensity as compared to the LSPR feature in the visible, as the thickness of the CeO_2 layers is increased. The $\frac{\Delta A}{A}$ spectra [Fig. 4(b)] show very broad LSPR-related absorption features. Figure 4(c) reports the imaginary part of the calculated polarizabilities for different values of the aspect ratio and of the dielectric constant of the medium. An aspect ratio smaller than one, which was considered in order to account for possible partial coalescence of NPs in the out-of-plane direction, significantly red-shifts the out-of-plane resonance above 450 nm, while a decrease in the dielectric constant of the medium blue-shifts the in-plane component to wavelengths below 600 nm. The observed marked absorption intensity at wavelengths between 450 nm and 650 nm in the sample with the thinnest CeO_2 spacer thickness can, therefore, be ascribed to a partially incomplete coverage of the NPs by the oxide, which may locally have a smaller dielectric constant than the bulk and which may induce a partial coalescence of Ag NPs in the out of plane direction. Indeed, also out-of-plane interparticle interactions, neglected in the calculations, are expected to increase with decreasing ceria spacer thickness, red-shifting the out-of-plane resonance (constructive interaction) and blue-shifting the in-plane resonance (destructive

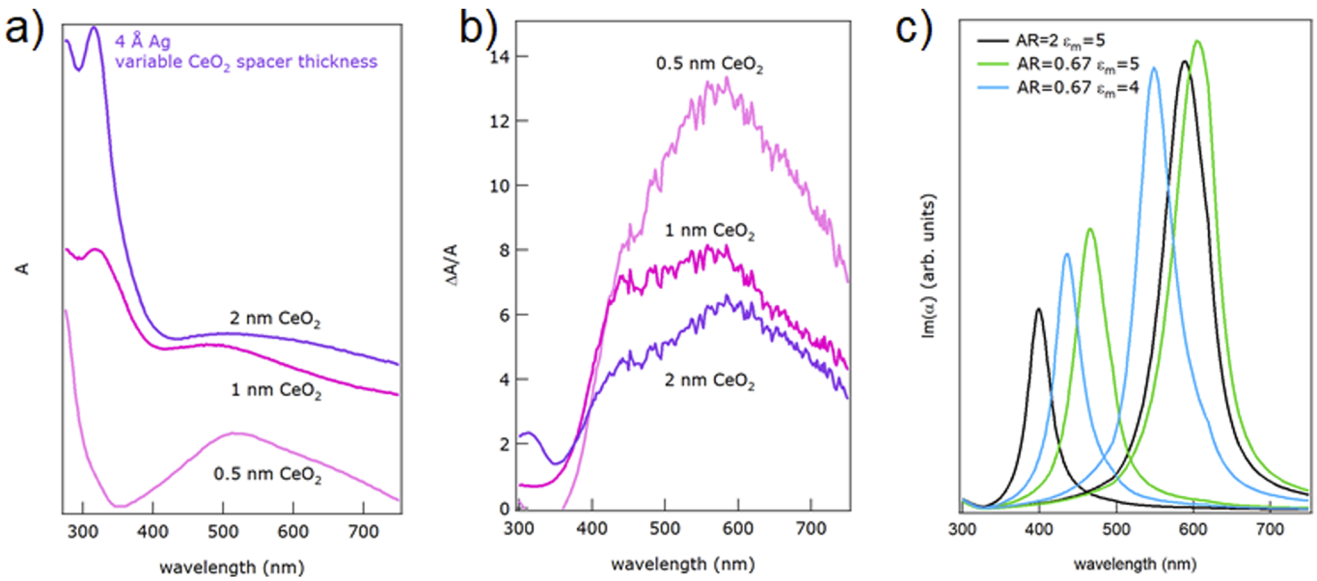

FIG. 4. (a) UV–Vis absorbance and (b) ΔA/A spectra of a 4 Å Ag embedded within CeO_2 layers of 0.5 nm, 1 nm, and 2 nm thickness; (c) the imaginary part of the calculated polarizability for Ag NPs of different aspect ratios embedded in a dielectric medium with different values of dielectric constant.

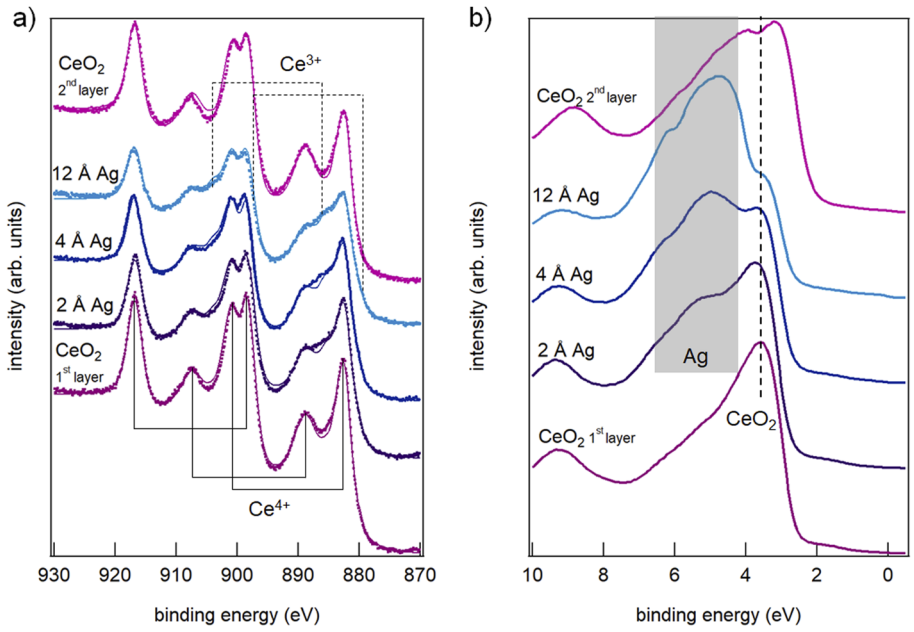

FIG. 5. (a) XPS Ce 3d and (b) UPS spectra acquired *in situ* at the different stages of the growth of a 12 Å Ag sample between two CeO_2 layers of 1 nm thickness.

interaction), thus possibly contributing to the more intense absorption between 450 nm and 650 nm in the sample with 0.5 nm CeO_2 spacer thickness.

Comparable changes in the LSPR energies were ascribed to modifications of the aspect ratio and of the oxide dielectric constant on other systems made of self-assembled Ag NPs embedded within metal oxides.[50]

In situ XPS/UPS analysis offers the possibility of investigating the electronic properties of the samples at the different stages of the growth and to obtain a more detailed description of the interaction between Ag NPs and CeO_2, interesting for a clearer understanding of the optical response. Figure 5 shows the XPS Ce 3d and UPS spectra acquired at different stages of the growth of a 12 Å Ag sample embedded between two CeO_2 layers of 1 nm thickness. After the deposition of the first CeO_2 layer, the Ce 3d spectrum [Fig. 5(a)] has the characteristic shape of Ce ions mainly in the 4+ oxidation state. The fitting of the spectra with Ce^{3+}- and Ce^{4+}-related components, as outlined in the section titled Experimental, indicates the additional presence of a minor, although non-negligible, concentration of Ce^{3+} ions (Table I), which are probably located at defect sites. A relatively large density of low-coordination sites is formed within the cerium oxide films due to the limited mobility of the adatoms during the growth, which is carried out at RT on a relatively rough magnesium oxide substrate, as compared to cerium oxide films grown on metal substrates in similar conditions and thermally treated in oxygen after the growth.[32,33] After the growth of 2 Å of Ag on the CeO_2 film, the Ce 3d XPS spectra show the appearance of features at 884 eV and 904 eV, ascribed to the most intense Ce^{3+} related doublet. The weight of such features progressively increases with the amount of deposited Ag, indicating an increasing concentration of Ce^{3+} ions. A dominant CeO_2 surface stoichiometry is restored after the growth of the topmost cerium oxide layer, showing that at least part of the NPs is covered by the cerium oxide film, which—in analogy with the first cerium oxide layer—is not expected to be fully stoichiometric. The Ce^{3+} concentration after each step of the growth, obtained by fitting the Ce 3d XPS spectra, is reported in Table I. A progressive reduction of comparable entity as the one observed here was already measured on epitaxial CeO_2 films grown on Pt(111) after the growth of Ag NPs,[21] and it was ascribed to a charge transfer from the NPs to the substrate, an effect often altering the properties of small nanoparticles coupled with oxides.[20] We note that the Ce^{3+} concentration increase that we measured after Ag growth (+10–15%) is possibly underestimated since the Ce^{3+} ions are expected to form at the bottom interface between the nanoparticles and the cerium film. For this reason, the Ce^{3+} related photoelectron intensity is expected to be more attenuated by the Ag NPs than the emission from Ce^{4+} ions, which are also present on the uncovered surface areas.

TABLE I. Ce^{3+} concentration evaluated from the fitting of Ce 3d XPS spectra.

Sample	$c_{Ce^{3+}}$ (%)
1 nm CeO_2	11 ± 2
1 nm CeO_2 + 2 Å Ag	20 ± 2
1 nm CeO_2 + 4 Å Ag	23 ± 2
1 nm CeO_2 + 12 Å Ag	26 ± 2
1 nm CeO_2 + 12 Å Ag + 1 nm CeO_2	9 ± 2

Previous works demonstrated small shifts of the LSPR with NP charging.[51,52] Although for the samples here investigated, it is quite difficult to quantify the expected shifts, we can hypothesize that the broadness of the observed plasmonic absorption features in the spectra of Figs. 3 and 4 may be ascribed not only to the relatively broad NP size distribution [see Fig. 1(b)] but also to the different interface

charge densities, which in turn depend on the NP size and on the nucleation site on the oxide surface. Moreover, modifications of the local polarizability of the oxide are expected to be induced by the charge transfer process.

The UPS spectrum of the CeO_2 film [Fig. 5(b), bottom spectrum] shows a dominant broad feature between 2 eV and 7 eV, which is due to emission from the valence band of O 2p character. The feature progressively changes shape with increasing amount of Ag deposited due to the appearance of features related to the Ag valence band at binding energies around 5 eV[53] and to the attenuation of the CeO_2-related main feature around 3 eV. After the growth of the topmost 1 nm thick CeO_2 layer [Fig. 5(b), topmost spectrum], the Ag-related features are still visible, demonstrating that the coverage of the Ag NPs is possibly not uniformly as thick as 1 nm, as expected given the size of the Ag NPs and the relatively rough surface morphology.

CONCLUSIONS

We show that Ag deposited by MBE on cerium oxide films with a non-ordered surface spontaneously aggregates into particles of nanometric size. If embedded within two cerium oxide films, the Ag NPs show an LSPR-related optical absorption band in the visible range, with a shape which changes as the amount of Ag deposited and the thickness of the CeO_2 dielectric are varied. The modifications of the optical absorbance are interpreted as due to variations in the NP aspect ratio, NP density, and dielectric constant of the oxide. Some charge transfer from the NPs to the oxide is observed and hypothesized to possibly affect the optical response.

SUPPLEMENTARY MATERIAL

See the supplementary material for the absorbance spectra of the MgO(001) substrate and of a 4 nm CeO_2 film supported on MgO(001), for the formula used to calculate the polarizability within the Maxwell Garnett model, and for the depolarization factors used for nanoparticles with a spheroidal shape and different aspect ratios.

ACKNOWLEDGMENTS

The present work is performed with the financial support of MIUR through PRIN (Project No. 2015CL3APH).

REFERENCES

[1] M. Melchionna and P. Fornasiero, ChemCatChem **9**, 3274 (2017).
[2] T. Montini, M. Melchionna, M. Monai, and P. Fornasiero, Chem. Rev. **116**, 5987 (2016).
[3] V. Bambagioni, C. Bianchini, Y. Chen, J. Filippi, P. Fornasiero, M. Innocenti, A. Lavacchi, A. Marchionni, W. Oberhauser, and F. Vizza, ChemSusChem **5**, 1266 (2012).
[4] R. Fiala, A. Figueroba, A. Bruix, M. Vaclavu, A. Rednyk, I. Khalakhan, M. Vorokhta, J. Lavkova, F. Illas, V. Potin, I. Matolinova, K. M. Neyman, and V. Matolin, Appl. Catal. B: Environ. **197**, 262 (2016).
[5] F. Lin, M. Rothensteiner, I. Alxneit, J. A. van Bokhoven, and A. Wokaun, Energy Environ. Sci. **9**, 2400 (2016).
[6] S. Guo, H. Arwin, S. N. Jacobsen, K. Järrendahl, and U. Helmersson, J. Appl. Phys. **77**, 5369 (1995).
[7] H. L. Tuller and A. S. Nowick, J. Electrochem. Soc. **126**, 209 (1979).
[8] A. Corma, P. Atienzar, H. García, and J.-Y. Chane-Ching, Nat. Mater. **3**, 394 (2004).
[9] Y. Li, Q. Sun, M. Kong, W. Shi, J. Huang, J. Tang, and X. Zhao, J. Phys. Chem. C **115**, 14050 (2011).
[10] A. Primo, T. Marino, A. Corma, R. Molinari, and H. García, J. Am. Chem. Soc. **133**, 6930 (2011).
[11] M. M. Khan, S. A. Ansari, D. Pradhan, D. H. Han, J. Lee, and M. H. Cho, Ind. Eng. Chem. Res. **53**, 9754 (2014).
[12] M. Kazazi, B. Moradi, and M. Delshad Chermahini, J. Mater. Sci.: Mater. Electron. **30**, 6116 (2019).
[13] L. Yue and X.-M. Zhang, J. Alloys Compd. **475**, 702 (2009).
[14] S. M. Kim, H. Lee, K. C. Goddeti, S. H. Kim, and J. Y. Park, J. Phys. Chem. C **119**, 16020 (2015).
[15] A. Tanaka, K. Hashimoto, and H. Kominami, J. Am. Chem. Soc. **134**, 14526 (2012).
[16] B. Li, T. Gu, T. Ming, J. Wang, P. Wang, J. Wang, and J. C. Yu, Acs Nano **8**, 8152 (2014).
[17] N. Wu, Nanoscale **10**, 2679 (2018).
[18] K. Wu, J. Chen, J. R. McBride, and T. Lian, Science **349**, 632 (2015).
[19] R. Long and O. V. Prezhdo, J. Am. Chem. Soc. **136**, 4343 (2014).
[20] Y. Lykhach, S. M. Kozlov, T. Skála, A. Tovt, V. Stetsovych, N. Tsud, F. Dvořák, V. Johánek, A. Neitzel, J. Mysliveček, S. Fabris, V. Matolín, K. M. Neyman, and J. Libuda, Nat. Mater. **15**, 284 (2015).
[21] P. Luches, F. Pagliuca, S. Valeri, F. Illas, G. Preda, and G. Pacchioni, J. Phys. Chem. C **116**, 1122 (2012).
[22] A. Bruix, J. A. Rodriguez, P. J. Ramírez, S. D. Senanayake, J. Evans, J. B. Park, D. Stacchiola, P. Liu, J. Hrbek, and F. Illas, J. Am. Chem. Soc. **134**, 8968 (2012).
[23] T. E. James, S. L. Hemmingson, T. Ito, and C. T. Campbell, J. Phys. Chem. C **119**, 17209 (2015).
[24] Y. Lykhach, A. Bruix, S. Fabris, V. Potin, I. Matolínová, V. Matolín, J. Libuda, and K. M. Neyman, Catal. Sci. Technol. **7**, 4315 (2017).
[25] J. A. Farmer and C. T. Campbell, Science **329**, 933 (2010).
[26] F. Benedetti, P. Luches, M. C. Spadaro, G. Gasperi, S. D'Addato, S. Valeri, and F. Boscherini, J. Phys. Chem. C **119**, 6024 (2015).
[27] J. S. Pelli Cresi, M. C. Spadaro, S. D'Addato, S. Valeri, S. Benedetti, A. Di Bona, D. Catone, L. Di Mario, P. O'Keeffe, A. Paladini, G. Bertoni, and P. Luches, Nanoscale **11**, 10282 (2019).
[28] P. Verma, Y. Kuwahara, K. Mori, and H. Yamashita, Catal. Today **324**, 83 (2019).
[29] C. T. Campbell, Surf. Sci. Rep. **27**, 1 (1997).
[30] M. Romeo, K. Bak, J. El Fallah, F. Le Normand, and L. Hilaire, Surf. Interface Anal. **20**, 508 (1993).
[31] T. Skála, F. Šutara, M. Škoda, K. C. Prince, and V. Matolín, J. Phys.: Condens. Matter **21**, 055005 (2009).
[32] P. Luches, F. Pagliuca, and S. Valeri, J. Phys. Chem. C **115**, 10718 (2011).
[33] P. Luches, F. Pagliuca, and S. Valeri, Phys. Chem. Chem. Phys. **16**, 18848 (2014).
[34] C. A. Schneider, W. S. Rasband, and K. W. Eliceiri, Nat. Methods **9**, 671 (2012).
[35] P. Luches, L. Giordano, V. Grillo, G. C. Gazzadi, S. Prada, M. Campanini, G. Bertoni, C. Magen, F. Pagliuca, G. Pacchioni, and S. Valeri, Adv. Mater. Interfaces **2**, 1500375 (2015).
[36] S. Eck, C. Castellarin-Cudia, S. Surnev, M. G. Ramsey, and F. P. Netzer, Surf. Sci. **520**, 173 (2002).
[37] J. L. Lu, H. J. Gao, S. Shaikhutdinov, and H. J. Freund, Surf. Sci. **600**, 5004 (2006).
[38] I. Simonsen, R. Lazzari, J. Jupille, and S. Roux, Phys. Rev. B **61**, 7722 (2000).
[39] C. Noguez, J. Phys. Chem. C **111**, 3806 (2007).
[40] H. Cha, D. Lee, J. H. Yoon, and S. Yoon, J. Colloid Interface Sci. **464**, 18 (2016).
[41] F. Illas and G. Pacchioni, J. Chem. Phys. **108**, 7835 (1998).
[42] F. Marabelli and P. Wachter, Phys. Rev. B **36**, 1238 (1987).
[43] S. D'Addato, D. Pinotti, M. C. Spadaro, G. Paolicelli, V. Grillo, S. Valeri, L. Pasquali, L. Bergamini, and S. Corni, Beilstein J. Nanotechnol. **6**, 404 (2015).

[44]M. Rycenga, C. M. Cobley, J. Zeng, W. Li, C. H. Moran, Q. Zhang, D. Qin, and Y. Xia, Chem. Rev. **111**, 3669 (2011).
[45]R. Lazzari, J. Jupille, and J.-M. Layet, Phys. Rev. B **68**, 045428 (2003).
[46]R. Lazzari and J. Jupille, Nanotechnology **23**, 135707 (2012).
[47]C. G. Granqvist and O. Hunderi, Phys. Rev. B **16**, 3513 (1977).
[48]E. D. Palik, *Handbook of Optical Constants of Solids* (Academic Press, San Diego, California, USA, 1985).
[49]F.-C. Chiu and C.-M. Lai, J. Phys. D: Appl. Phys. **43**, 075104 (2010).
[50]L. Pascua, F. Stavale, N. Nilius, and H.-J. Freund, J. Appl. Phys. **119**, 095310 (2016).
[51]M. Zapata Herrera, J. Aizpurua, A. K. Kazansky, and A. G. Borisov, Langmuir **32**, 2829 (2016).
[52]S. Benedetti, I. Valenti, and S. Valeri, J. Phys. Chem. C **123**, 8206 (2019).
[53]K. Ozawa, T. Sato, M. Kato, K. Edamoto, and Y. Aiura, J. Phys. Chem. B **109**, 14619 (2005).